ARTICLE

Bulk Heterojunction Polymer Memory Devices with Reduced Graphene Oxide as Electrodes

Juqing Liu,[†,⊥] Zongyou Yin,[‡,⊥] Xiehong Cao,[‡] Fei Zhao,[†] Anping Lin,[†] Linghai Xie,[†,*] Quli Fan,[†] Freddy Boey,[‡,§] Hua Zhang,[‡,§,*] and Wei Huang[†,*]

[†]Key Laboratory for Organic Electronics & Information Displays (KLOEID) and Institute of Advanced Materials (IAM), Nanjing University of Posts and Telecommunications, 9 Wenyuan Road, Nanjing 210046, China, [‡]School of Materials Science and Engineering, Nanyang Technological University, 50 Nanyang Avenue, Singapore 639798, Singapore, and [§]Centre for Biomimetic Sensor Science, Nanyang Technological University, 50 Nanyang Drive, Singapore 637553, Singapore. [⊥]These authors contributed equally to this work.

ABSTRACT A unique device structure with a configuration of reduced graphene oxide (rGO) /P3HT:PCBM/Al has been designed for the polymer nonvolatile memory device. The current−voltage (*I*−*V*) characteristics of the fabricated device showed the electrical bistability with a write-once-read-many-times (WORM) memory effect. The memory device exhibits a high ON/OFF ratio (10^4−10^5) and low switching threshold voltage (0.5−1.2 V), which are dependent on the sheet resistance of rGO electrode. Our experimental results confirm that the carrier transport mechanisms in the OFF and ON states are dominated by the thermionic emission current and ohmic current, respectively. The polarization of PCBM domains and the localized internal electrical field formed among the adjacent domains are proposed to explain the electrical transition of the memory device.

KEYWORDS: polymer memory · bulk heterojunction · write-once-read-many-times · reduced graphene oxide · sheet resistance

As one of the emerging memory technologies, the organic memory (electrical bistable) device, with a typical configuration of organic active materials sandwiched between two electrodes, has attracted increasing interest due to its role in organic electronics comprising simple structure, low cost, large-capacity data storage, *etc*. Two important components of memory devices are the organic active materials and conducting electrodes. Recently, many kinds of organic active materials, including small molecules,[1,2] polymers,[3] redox metal complexes[4] and hybrid organic/inorganic nanocomposites,[5−9] have been used for memory devices, with Al, Cu, indium−tin oxide (ITO), and p- or n-doped Si as the most widely used electrodes. Among these memory devices, the polymer-based nanocomposites, including metal or metal oxide nanoparticles[6,7] and carbon-based nanomaterials,[5,8,9] have shown particular interest as nanomaterials normally act as the charge acceptors to realize the memory effect. Although the poly(3-hexyl thiophene) (P3HT) and methanofullerene [6,6]-phenyl C61-butyric acid methyl ester (PCBM) bulk-heterojunction (BHJ) composites, a promising system of electron donors and acceptors, were used for the energy conversion,[10,11] few studies on the electrical bistable behaviors of this BHJ composites have been reported until now.

On the other hand, a proper substitute for ITO and other metal electrodes is required during the fabrication of memory devices, due to the shortcomings of normally used electrodes, such as the brittle nature, high cost, and limit amount of the element in the earth, *etc*. Meanwhile, the work function, sheet resistance, and chemical stability of electrode materials greatly affect the electrical properties of memory devices.[12−15] For example, the current−voltage (*I*−*V*) characteristics of memory devices are affected by the charge injection barrier, which is dependent on the work functions of electrodes and the energy levels of organic materials. Therefore, how to choose the appropriate electrode materials is very important in the design of memory devices. If the flexible conducting polymer electrode is used, its high sheet resistance normally induces a high switching voltage in the memory device.[13] In addition, the chemical stability of electrodes will directly affect the *I*−*V* properties and memory effects of devices. For example, the copper-doping in the organic active layer during deposition can induce a hysteresis phenomenon, which, however, was not observed in Al electrodes because of no Al nanoparticles penetrating into the organic materials.[16,17]

Graphene is a promising conductive material due to its extremely high carrier

*Address correspondence to wei-huang@njupt.edu.cn, iamlhxie@njupt.edu.cn, hzhang@ntu.edu.sg.

Received for review April 25, 2010 and accepted June 03, 2010.

Published online June 11, 2010.
10.1021/nn100877s

© 2010 American Chemical Society

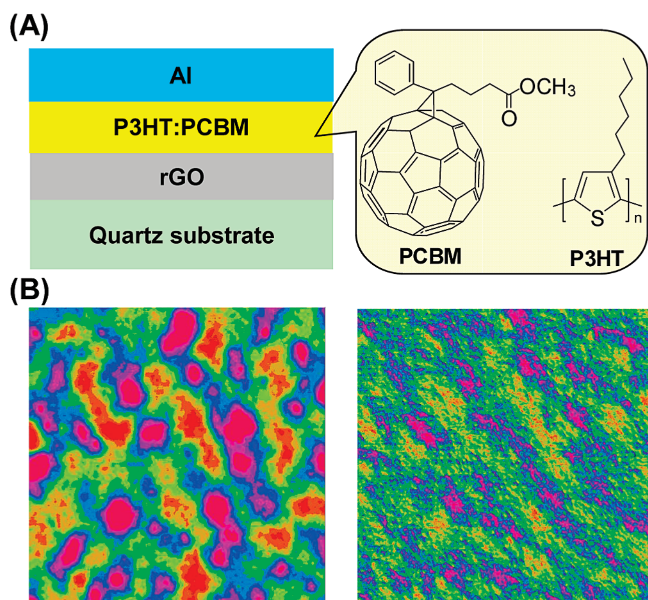

Figure 1. (A) Schematic diagram of the configuration of memory device (rGO/P3HT:PCBM/Al) and the chemical structures of P3HT and PCBM. (B) Tapping-mode AFM topographic (left) and phase (right) images of P3HT:PCBM layer on rGO film. Figure size = 2.0 × 2.0 μm². Z scale for topographic (left) and phase (right) images is 20 nm and 20°, respectively.

mobility, high chemical stability, and flexibility. Various approaches including micromechanical cleavage,[18] epitaxial growth,[19,20] solvothermal synthesis,[21] and liquid-phase exfoliation,[22−24] have been proposed to prepare graphene, but these methods face the challenges of low cost, high yield, and large-amount production. Currently, the grahene oxide (GO) reduced by thermal annealing, which is so far one of the most efficient and effective methods to produce reduced GO (rGO), is used as electrodes in solar cells, organic light-emitting diodes, and electronic devices.[25−28] In this contribution, we demonstrate that the rGO film can serve as a conductive electrode in the BHJ polymer memory device, which exhibits a write-once-read-many-times (WORM)

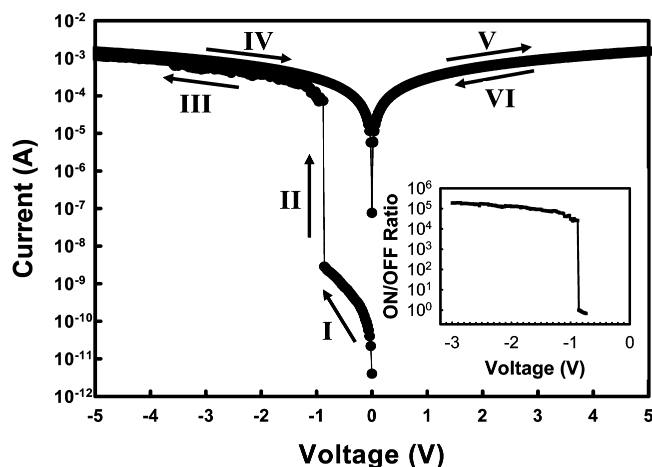

Figure 2. The $I-V$ characteristics of the rGO/P3HT:PCBM/Al device. The sheet resistance of rGO electrode is ~2.4 kΩ/sq (device 2 in Table 1). Inset: the ON/OFF ratio as a function of applied voltage in the negative sweep.

memory effect. In addition, the carrier transport mechanism of the memory device is proposed, and its electrical transition from a low conductivity state (OFF state) to a high conductivity state (ON state) is discussed.

The polymer memory device with the BHJ active layer and rGO electrode was fabricated on quartz. Briefly, the GO thin film was spin-coated on the precleaned quartz. Its thickness was adjusted by the spin-coating condition. To improve the electrical conductivity of the electrode, GO film was reduced by the high temperature annealing and the conducting rGO film was obtained. Subsequently, a P3HT:PCBM functional layer was spin-coated onto the top of rGO film to realize the memory effect. Finally, a top Al electrode was coated by thermal evaporation under vacuum. Figure 1A shows the schematic diagram of the fabricated memory, referred to as rGO/P3HT:PCBM/Al, and the chemical structures of P3HT and PCBM. Figure 1B shows the AFM images of the obtained P3HT:PCBM film, where the topography and phase images clearly reveal the formation of aggregated domains of PCBM in the P3HT matrix after thermal annealing treatment, which is consistent with the previous report.[29]

The memory effect was observed from the characteristic $I-V$ curves of the rGO/P3HT:PCBM/Al device (Figure 2). Initially, the conductivity of the as-fabricated device is low (defined as the OFF state). The current increased progressively after applying the negative bias (stage I), varying in a range of approximately 10^{-12} to 10^{-9} A. When a switching threshold voltage of −0.9 V was applied (stage II), the current increases dramatically from 10^{-9} to 10^{-5} A, indicating the transition of the diode from a low conductivity state (OFF state) to a high conductivity state (ON state), with an ON/OFF current ratio of 10^4 (inset in Figure 1). This transition from the OFF to ON state is equivalent to the "writing" process, and the high ON/OFF current ratio promises a low misreading probability in the memory operation.[30] After the electronic transition, the device remains in the ON state during the subsequent negative voltage scan (stages III and IV), even if the power is turned off. This promises the nonvolatile nature of the memory effect. The current in the ON state is in the range of $10^{-7}-10^{-3}$ A with the sweeping voltages from −5 to 5 V. One of the most impressive features of the fabricated device is that the high conductivity does not go back to the low one by applying a reverse voltage scan (stage V), and a similar phenomenon is observed in the subsequent scan (stage VI). Therefore, this device exhibits the WORM type memory effect. Note that the role of PCBM molecules is very important in the fabricated memory device. Without PCBM, the $I-V$ curves do not exhibit the electrical bistable phenomenon, indicating that the WORM effect of the BHJ device is attributed to the existence of PCBM.

To clarify the effect of sheet resistance of rGO film on the device performance, we have characterized the

TABLE 1. Sheet Resistances of rGO Films and the Performance of Fabricated Polymer Memory Devices. The *I*−*V* Curves of Device 2 Are Shown in Figure 2

device	sheet resistance (kΩ/sq)	switching voltage (V)	current in OFF state (A)	current in ON state (A)	ON/OFF ratio
1	~10.0	1.2	5.1×10^{-9}	6.2×10^{-5}	1.2×10^{4}
2	~2.4	0.9	2.8×10^{-9}	7.3×10^{-5}	2.2×10^{4}
3	~0.3	0.5	5.7×10^{-10}	2.2×10^{-4}	4×10^{5}

I−*V* properties of the rGO/P3HT:PCBM/Al devices with different rGO electrodes. It was found that the switching behavior of all memory devices is similar to that in Figure 2, and all devices exhibited the WORM effect. On the basis of our experimental results, the summary of sheet resistance of rGO film, switching voltage, current in ON and OFF state, and ON/OFF ratio of the measured devices is listed in Table 1. Obviously, the switching voltage decreases with the decrease of sheet resistance of rGO film. Normally, the electrode with a high sheet resistance will lower the carrier injection and increase the switching voltage in organic memories.[13] In our study, the lower sheet resistance of rGO film enhances the carrier injection efficiency from rGO electrode to BHJ. Therefore, the switching threshold voltage increases in the device with a higher sheet resistance rGO electrode. This phenomenon might be attributed to the fact that the current in OFF state is limited under the low injection efficiency. Furthermore, the increase of ON state current and decrease of OFF state current result in the increased ON/OFF current ratio, which is particularly obvious in the devices with a lower sheet resistance of rGO electrode (Table 1).

To understand the carrier transport mechanism in the WORM memory device, the experimental *I*−*V* data and fitted data in the ON and OFF states are studied for device 2 (Table 1), Figure 3. In the OFF state, the plot of ln(*I*) *vs* $V^{1/2}$ in the sweeping voltage ranging from 0.06 to 0.9 V before the electrical transition can be fitted to a straight line with eq 1,[31] Figure 3A.

$$I \propto AT^2 \exp\left[\frac{-(\phi - q\sqrt{qV/4d\pi\varepsilon})}{kT}\right] \qquad (1)$$

where *I* and *V* are the device current and applied voltage, respectively; *A*, *T*, *k*, ϕ, *q*, *d*, π, and ε are the Richardson constant, temperature, Boltzmann constant, Schottky energy barrier, electron charge, BHJ film thickness, ratio of circumference to diameter, and electric constant, respectively. Such a linearity characteristic suggests that the carrier transport mechanism in the OFF state is dominated by the thermionic emission, and the conduction mechanism is dominated by the charge injection from electrodes.

In the ON state from −5 to −0.02 V after the conductive switching, the experimental data of the rGO/P3HT:PCBM/Al device, shown in the plot of ln(*I*) *vs* ln(*V*) (Figure 3B), were fitted with eq 2.[31]

$$I \propto V \exp\left(\frac{-\Delta E_{ae}}{kT}\right) \qquad (2)$$

where *I* and *V* are the device current and applied voltage, respectively; ΔE_{ae}, *T*, and *k* are the activation energy of electron, temperature, and Boltzmann constant, respectively. The obtained slope (1.02) is nearly equal to 1, indicating that the ohmic conduction dominates the carrier transport process.[31] Since the *I*−*V* behaviors for the positive (stage V) and reverse (stage VI) voltage sweeping between 0 and 5 V are very similar to those (stage IV) from 0 to −5 V, as shown in Figure 2, the carrier transport mechanism in the ON state is the ohmic process. Meanwhile, the ohmic process promises the

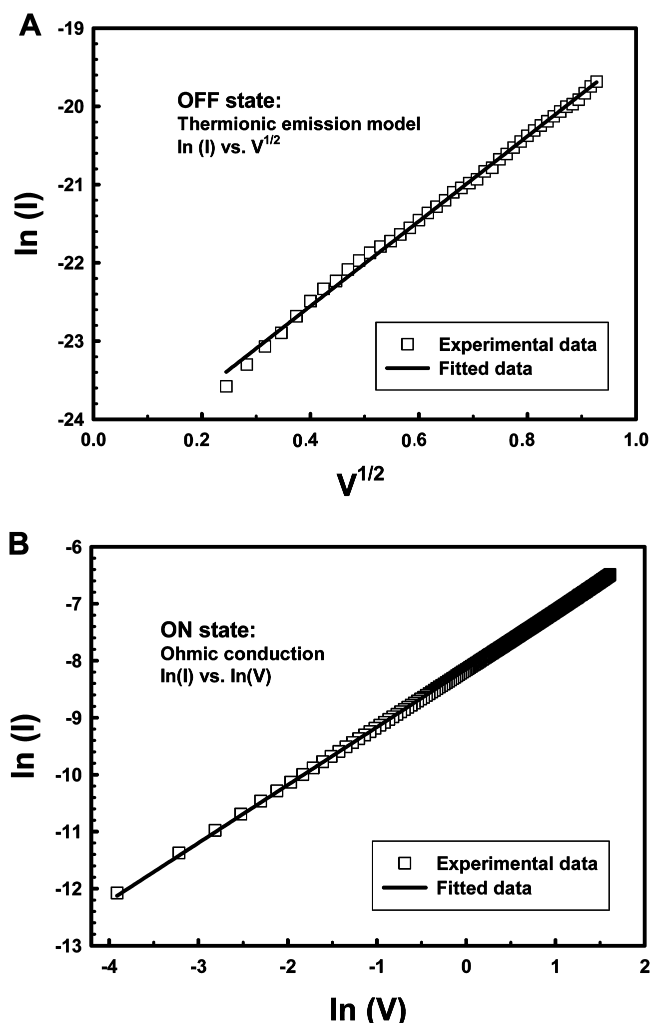

Figure 3. Experimental results and theoretical fitted data of the *I*−*V* curves for the rGO/P3HT:PCBM/Al device (*i.e.*, device 2 in Table 1) in (A) OFF state (low conductivity) and (B) ON state (high conductivity).

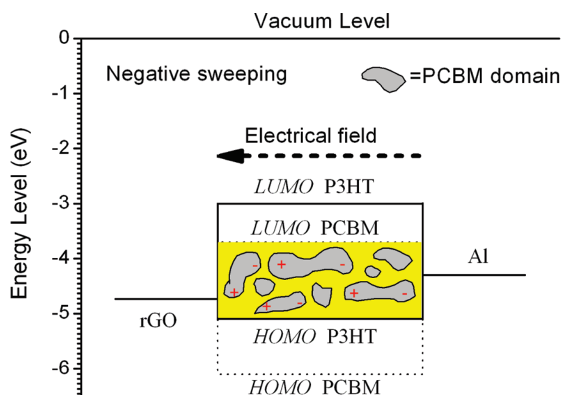

Figure 4. The energy band diagrams of the rGO/P3HT: PCBM/Al device and a schematic illustration of the polarization of PCBM domains in P3HT matrix under an applied electrical field.

absence of captured carriers due to the trap-free polymer, fullerene devices,[32] which is quite different from the hybrid organic/inorganic nanocomposites and PCBM-based memories.[8,33−35] In these memory devices, nanocomposites normally act as the charge traps to realize the electrical switching and memory effect. For example, the dominated factor to affect the ON state current is probably the space-charge-limited-current for the polystyrene−Au nanoparticle system,[33] Poole−Frenkel emission for the polystyrene−PCBM system,[8] and Fowler−Nordheim tunneling for polyimide-$Ni_{1-x}Fe_x$ nanoparticle system.[34]

On the basis of the aforementioned discussion, we propose that the electrical switching behavior is attributed to the field-induced polarization of PCBM domains. Figure 4 shows the energy band diagrams of the fabricated rGO/P3HT:PCBM/Al device and a schematic illustration of polarization in PCBM domains in P3HT matrix. The work function of rGO film measured by Kelvin probe force microscopy (KPFM) is −4.7 eV, which is comparable to the values (−4.88 eV) of chemically reduced GO film.[36] The work function of Al is −4.3 eV. The highest occupied molecular orbital (HOMO) and lowest unoccupied molecular orbital (LUMO) are −5.2 and −3.0 eV for P3HT and −6.1 and −3.7 eV for PCBM, respectively. This indicates a large electron-injection barrier (1.0 eV) and hole-injection barrier (0.9 eV) under the applied negative voltage. The large barrier results in the low injection efficiency at the first negative sweeping, resulting in the thermionic emission in the OFF state. The thermionic emission dominates the carrier transport process until the applied voltage approaches the switching voltage. Normally, the thermal annealing can introduce the formation of PCBM domains,[37−39] resulting in the discontinuity of PCBM-rich phase in matrix. Therefore, the P3HT:PCBM composites are illustrated as two dielectric phases with a dielectric constant of 3.9 for PCBM[40] and 3 for P3HT.[41] The formed PCBM domains in the P3HT matrix can be polarized under an applied electrical field.[42] The phenomenon should be more distinct under the low charge injection efficiency. The polarization of PCBM domains leads to the increase of the localized internal electrical field among the adjacent domains and induces the conductive switching.[43] Meanwhile, the polarized states and the localized internal electrical fields are maintained, even when the power is turned off due to the nonvolatile properties of devices. In the previous reports, the switching behavior was explained by the metal filament model for P3HT-based memory devices[14] and the field-induced charge transfer for PCBM-based memory devices,[8,35] but the former memory exhibits the erasing operation under a reverse bias applied and a high ON state current of $10^{-2}-10^{-1}$ A, and the latter memory shows the erasing operation due to the detrapping of trapped charges under an external electrical field. Therefore, the models of metal filament and field-induced charge transfer cannot be used to explain our results.

In summary, an electrical bistable device with the configuration of rGO/P3HT:PCBM/Al has been demonstrated. The $I-V$ curves for the devices show the electrical bistable behavior, a WORM memory effect, and the dependence of switching threshold voltage on the sheet resistance of rGO electrodes. The carrier transport mechanism based on the experimental and fitted data of $I-V$ curves indicates an electrical transition from the charge injection limited current in the OFF state to the ohmic current in the ON state. Such transition might be attributed to the polarization of PCBM domains and the formation of a localized internal electrical field among the adjacent domains. Because of the nonvolatile and inerasable features, the WORM memory devices have potential applications in the archival storages and databases, in which the information has to be reliably kept and capable of being stored permanently. Meanwhile, WORM memory could also be used as electronic labels and radio frequency identification (RFID).

MATERIALS AND METHODS

Preparation of Reduced Graphene Oxide (rGO) Film. Graphene oxide (GO) was prepared by the modified Hummers method.[44,45] GO power was obtained by drying the GO suspension in vacuum for a week. Exfoliated GO was dispersed in methanol by ultrasonication. The quartz was sonicated in DI-water with subsequent cleaning in piranha solution (H_2SO_4:30 wt % H_2O_2 = 3:1) at 110 °C for 1 h. After the cleaned quartz was thoroughly rinsed with Milli-Q water and dried with N_2 gas, the dispersed GO solution was spin-coated on its surface at 4000 rpm. The thickness of GO film can be adjusted by controlling the spin-coating conditions. The produced GO film was then annealed at 1000 °C under the mixture of Ar_2 and H_2 for 2 h to obtain the conductive rGO film.

Fabrication of Polymer Memory Devices. Polymer memory devices were fabricated on the rGO film-coated quartz substrates. The active layer is the bulk heterojunction (BHJ) composites of P3HT and PCBM (w/w = 1:1). First, the BHJ composites were spin-coated onto the top of rGO film at 700 rpm and then annealed

at 150 °C for 15 min under N_2 atmosphere, producing a 200 nm BHJ film. Then a 60 nm top Al electrode, with an active area of ~6 mm^2, was thermally evaporated under the vacuum of ~10^{-6} mbar. Before measurement, the as-fabricated device was annealed again at 150 °C for 15 min under N_2 atmosphere.

Characterization. The AFM images were obtained by using a Dimension 3100 (Veeco, CA) in tapping mode with a Si tip (resonance frequency: 320 kHz; spring constant: 42 N m^{-1}) at a scanning rate of 1 Hz. The work function was measured by KPFM (KP technology Ltd., Caithness, UK) in air based on the contact potential difference between the sample and the reference Au electrodes. The $I-V$ measurements were performed by using a Hewlett-Packard 4156B semiconductor parameter analyzer under ambient conditions. The sheet resistance was measured by a four-probe instrument.

Acknowledgment. The authors gratefully acknowledge the financial support from the "973" project (2009CB930600), NNSFC (Grants 20704023, 60876010, 60706017, and 20774043), the Key Project of Chinese Ministry of Education (No. 208050, 707032, NCET-07-0446), the NSF of Jiangsu Province (Grants 07KJB150082, BK2008053, 08KJB510013, SJ209003and TJ207035), the Research Fund for Postgraduate Innovation Project of Jiangsu Province (CX08B_083Z) and STTTP (No. 2009120). H.Z. acknowledges the following support: AcRF Tier 1 (RG 20/07) from MOE, CRP (NRF-CRP2-2007-01) from NRF, A*STAR SERC Grants (No. 092 101 0064) from A*STAR, and the Centre for Biomimetic Sensor Science at NTU in Singapore.

REFERENCES AND NOTES

1. Collier, C. P.; Mattersteig, G.; Wong, E. W.; Luo, Y.; Beverly, K.; Sampaio, J.; Raymo, F. M.; Stoddart, J. F.; Heath, J. R. A [2]Catenane-Based Solid State Electronically Reconfigurable Switch. *Science* **2000**, *289*, 1172–1175.
2. Shang, Y.; Wen, Y.; Li, S.; Du, S.; He, X.; Cai, L.; Li, Y.; Yang, L.; Gao, H.; Song, Y. A Triphenylamine-Containing Donor−Acceptor Molecule for Stable, Reversible, Ultrahigh Density Date Storage. *J. Am. Chem. Soc.* **2007**, *129*, 11674–11675.
3. Xie, L.; Ling, Q.; Hou, X.; Huang, W. An Effective Friedel−Crafts Postfunctionization of Poly(*N*-Vinylcarbazole) to Tune Carrier Transportation of Supramolecular Organic Semiconductors Based on π-Stacked Polymers for Nonvolatile Flash Memory Cell. *J. Am. Chem. Soc.* **2008**, *130*, 2120–2121.
4. Ling, Q.; Song, Y.; Ding, S.; Zhu, C.; Chan, D. S. H.; Kwong, D.; Kang, E. T.; Neoh, K. G. Nonvolatile Polymer Memory Device Based on a Novel Copolymer of *N*-Vinylcarbazole and Eu-Complexed Vinylbenzoate. *Adv. Mater.* **2005**, *17*, 455–459.
5. Liu, G.; Ling, Q.; Teo, E. Y. H.; Zhu, C.; Chan, D. S.; Neoh, K.; Kang, E. T. Electrical Conductance Tuning and Bistable Switching in Poly(*N*-Vinylcarbazole)-Carbon Nanotube Composite Films. *ACS Nano* **2009**, *3*, 1929–1937.
6. Tseng, R. J.; Huang, J.; Ouyang, J. Y.; Kaner, R. B.; Yang, Y. Polyaniline Nanofiber/Gold Nanoparticle Nonvolatile Memory. *Nano Lett.* **2005**, *5*, 1077–1080.
7. Yun, D. Y.; Kwak, J. K.; Jung, J. H.; Kim, T. W.; Son, D. Electrical Bistabilities and Carrier Transport Mechanisms of Write-Once-Read-Many-Times Memory Devices Fabricated Utilizing ZnO Nanoparticles Embedded in a Polystyrene Layer. *Appl. Phys. Lett.* **2009**, *95*, 143301.
8. Chu, C. W.; Ouyang, J. Y.; Tseng, J. H.; Yang, Y. Organic Donor-−Acceptor System Exhibiting Electrical Bistability for Use in Memory Devices. *Adv. Mater.* **2005**, *17*, 1440–1443.
9. Majumdar, H. S.; Baral, J. K.; Österbacka, R.; Ikkala, O.; Stubb, H. Fullerene-Based Bistable Devices and Associated Negative Differential Resistance Effect. *Org. Electron.* **2005**, *6*, 188–192.
10. Padinger, F.; Rittberger, R. S.; Sariciftci, N. S. Effects of Postproduction Treatment on Plastic Solar Cells. *Adv. Funct. Mater.* **2003**, *13*, 85–88.
11. Lenes, M.; Shelton, S. W.; Sieval, A. B.; Kronholm, D. F.; Hummelen, J. C.; Blom, P. W. M. Electron Trapping in Higher Adduct Fullerene-Based Solar Cells. *Adv. Funct. Mater.* **2009**, *19*, 3002–3007.
12. Ling, Q.; Song, Y.; Lim, S.; Teo, C. E.; Tan, Y.; Zhu, C.; Chan, D. S. H.; Kwong, D.; Kang, E.; Neoh, K. A Dynamic Random Access Memory Based on a Conjugated Copolymer Containing Electron-Donor and -Acceptor Moieties. *Angew. Chem., Int. Ed.* **2006**, *45*, 2947–2951.
13. Li, L.; Ling, Q.; Lim, S. L.; Tan, Y.; Zhu, C.; Chan, D. S. H.; Kang, E. T.; Neoh, K. G. A Flexible Polymer Memory Device. *Org. Electron.* **2007**, *8*, 401–406.
14. Joo, W. -J.; Choi, T. -L.; Lee, J.; Lee, S. K.; Jung, M.; Kim, N.; Kim, J. M. Metal Filament Growth in Electrically Conductive Polymers for Nonvolatile Memory Application. *J. Phys. Chem. B* **2006**, *110*, 23812–23816.
15. Liu, J.; Chen, S.; Chen, L.; Xie, L.; Qian, Y.; Ling, Q.; Huang, W. Organic/Polymeric Memory and Their Switching Mechanisms. *Chin. Sci. Bull. (Chin. Ver.)* **2009**, *54*, 3420–3432.
16. Chiguvare, Z.; Parisi, J.; Dyakonov, V. Current Limiting Mechanisms in Indium-Tin-Oxide/Poly-3-Hexylthiophene/Aluminum Thin Film Devices. *J. Appl. Phys.* **2003**, *94*, 2440–2448.
17. Baral, J. K.; Majumdar, H. S.; Laiho, A.; Jiang, H.; Kauppinen, E. I.; Ras, R. H.; Ruokolainen, J.; Ikkala, O.; Österbacka, R. Organic Memory Using [6,6]-Phenyl-C61 Butyric Acid Methyl Ester: Morphology, Thickness, and Concentration Dependence Studies. *Nanotechnology* **2008**, *19*, 035203.
18. Novoselov, K. S.; Geim, A. K.; Morozov, S. V.; Jiang, D.; Zhang, Y.; Dubonos, S. V.; Grigorieva, I. V.; Firsov, A. A. Electric Field Effect in Atomically Thin Carbon Films. *Science* **2004**, *306*, 666–669.
19. Berger, C.; Song, Z. M.; Li, X. B.; Wu, X. S.; Brown, N.; Naud, C.; Mayou, D.; Li, T.; Hass, J.; Marchenkov, A. N.; *et al.* Electronic Confinement and Coherence in Patterned Epitaxial Graphene. *Science* **2006**, *312*, 1191–1196.
20. Sutter, P. W.; Flege, J. I.; Sutter, E. A. Epitaxial Graphene on Ruthenium. *Nat. Mater.* **2008**, *7*, 406–411.
21. Choucair, M.; Thordarson, P.; Stride, J. A. Gram-Scale Production of Graphene Based on Solvothermal Synthesis and Sonication. *Nat. Nanotechnol.* **2009**, *4*, 30–33.
22. Hernandez, Y.; Nicolosi, V.; Lotya, M.; Blighe, F. M.; Sun, Z.; De, S.; McGovern, I.; Holland, B.; Byrne, M.; Gun'ko, Y.; Boland, J.; *et al.* High Yield Production of Graphene by Liquid Phase Exfoliation of Graphite. *Nat. Nanotechnol.* **2008**, *3*, 563–568.
23. Lotya, M.; Hernandez, Y.; King, P. J.; Smith, R. J.; Nicolosi, V.; Karlsson, L. S.; Blighe, F. M.; De, S.; Wang, Z. M.; McGovern, I. T.; *et al.* Liquid Phase Production of Graphene by Exfoliation of Graphite in Surfactant/Water Solutions. *J. Am. Chem. Soc.* **2009**, *131*, 3611–3620.
24. Blake, P.; Brimicombe, P. D.; Nair, R. R.; Booth, T. J.; Jiang, D.; Schedin, F.; Ponomarenko, L. A.; Morozov, S. V.; Gleeson, H. F.; Hill, E. W.; *et al.* Graphene-Based Liquid Crystal Device. *Nano Lett.* **2008**, *8*, 1704–1708.
25. Yin, Z.; Wu, S.; Zhou, X.; Huang, X.; Zhang, Q.; Boey, F.; Zhang, H. Electrochemical Deposition of ZnO Nanorods on Transparent Reduced Graphene Oxide Electrodes for Hybrid Solar Cells. *Small* **2010**, *6*, 307–312.
26. Wu, J.; Agrawal, M.; Becerril, H. A.; Bao, Z.; Liu, Z.; Chen, Y. S.; Peumans, P. Organic Light-Emitting Diodes on Solution-Processed Graphene Transparent Electrodes. *ACS Nano* **2010**, *4*, 43–48.
27. Li, B.; Cao, X.; Ong, H. G.; Cheah, J. W.; Zhou, X.; Yin, Z.; Li, H.; Wang, J.; Boey, F.; Huang, W.; *et al.* All-Carbon Electronic Devices Fabricated by Directly Grown Single-Walled Carbon Nanotubes on Reduced Graphene Oxide Electrodes. *Adv. Mater.*, DOI: 10.1002/adma.201000736.
28. He, Q.; Sudibya, H. G.; Yin, Z.; Wu, S.; Li, H.; Boey, F.; Huang, W.; Chen, P.; Zhang, H. Centimeter-Long and Large-Scale Micropatterns of Reduced Graphene Oxide Films: Fabrication and Sensing Applications. *ACS Nano*, DOI: 10.1021/nn100780v.

29. Moulé, A. J.; Meerholz, K. Controlling Morphology in Polymer-Fullerene Mixtures. *Adv. Mater.* **2008**, *20*, 240–245.
30. Ling, Q.; Song, Y.; Teo, C. E.; Lim, S.; Zhu, C.; Chan, D. S. H.; Kwong, D.; Kang, E.; Neoh, K. WORM-Type Memory Device Based on a Conjugated Copolymer Containing Europium Complex in the Main Chain. *Electronchem. Solid-State Lett.* **2006**, *9*, 268–271.
31. Sze, S. M. *Physics of Semiconductor Devices*; Wiley: New York, 1981.
32. Lenes, M.; Wetzelaer, G. A. H.; Kooistra, F. B.; Veenstra, S. C.; Hummelen, J. C.; Blom, P. W. M. Fullerene Bisadducts for Enhanced Open-Circuit Voltages and Efficiencies in Polymer Solar Cells. *Adv. Mater.* **2008**, *20*, 2116–2119.
33. Lin, H. -T.; Pei, Z.; Chan, Y. -J. Carrier Transport Mechanism in a Nanoparticle-Incorporated Organic Bistable Memory Device. *IEEE Electron Dev. Lett.* **2007**, *28*, 569–571.
34. Kim, T. W.; Jung, J. H.; Yoon, C. S.; Kim, Y. -H. Multilevel Charging and Discharging Mechanisms of Vertically Stacked $Ni_{1-x}Fe_x$ Self-Assembled Nanoparticle Arrays Embedded in Polyimide Layers. *Appl. Phys. Lett.* **2008**, *92*, 042103.
35. Liu, Z.; Xue, F.; Su, Y.; Varhramyan, K. Electrically Bistable Memory Device Based on Spin-Coated Molecular Complex Thin Film. *IEEE Electron Dev. Lett.* **2006**, *27*, 151–153.
36. Kong, B. S.; Geng, J.; Jung, H. T. Layer-by-Layer Assembly of Graphene and Gold Nanoparticles by Vacuum Filtration and Spontaneous Reduction of Gold Ions. *Chem. Commun.* **2009**, 2174–2176.
37. Li, L.; Lu, G.; Li, S.; Tang, H.; Yang, X. Epitaxy-Assisted Creation of PCBM Nanocrystals and Its Application in Constructing Optimized Morphology for Bulk-Heterojunction Polymer Solar Cells. *J. Phys. Chem. B* **2008**, *112*, 156651–156658.
38. Swinnen, A.; Haeldermans, I.; vande Ven, M.; D'Haen, J.; Vanhoyland, G.; Aresu, S.; D'Olieslaeger, M.; Manca, J. Tuning the Dimensions of C_{60}-Based Needlelike Crystals in Blended Thin Films. *Adv. Funct. Mater.* **2006**, *16*, 760–765.
39. Beal, R. M.; Stavrinadis, A.; Warner, J. H.; Smith, J. M.; Assender, H. E.; Watt, A. R. The Molecular Structure of Polymer-Fullerene Composite Solar Cells and Its Influence on Device Performance. *Macromolecules* **2010**, *43*, 2343–2348.
40. Blom, P. W. M.; Mihailetchi, V. D.; Koster, L. J. A.; Markow, D. E. Device Physics of Polymer:Fullerene Bulk Heterojunction Solar Cells. *Adv. Mater.* **2007**, *19*, 1551–1566.
41. Juška, G.; Genevičius, K.; Österbacka, R.; Arlauskas, K.; Kreouzis, T.; Bradley, D. D. C.; Stubb, H. Initial Transport of Photogenerated Charge Carriers in π-Conjugated Polymers. *Phys. Rev. B* **2003**, *67*, 081201.
42. Sliauzys, G.; Juska, G.; Genevicius, K.; Arlauskas, K.; Dennler, G. Charge Polarization in Annealed Bulk-Heterojunction Solar Cell. *Thin Solid Films* **2008**, *516*, 7230–7233.
43. Laiho, A.; Himadri, S.; Majumdar, S.; Baral, J. K. ; Jansson, F.; Österbacka, R. Ikkala. Tuning The Electrical Switching of Polymer Fullerene Nanocomposite Thin Film Devices by Control of Morphology. *Appl. Phys. Lett.* **2008**, *93*, 203309.
44. Hummers, W. S.; Offeman, R. E. Preparation of Graphitic Oxide. *J. Am. Chem. Soc.* **1958**, *80*, 1339.
45. Zhou, X.; Huang, X; Qi, X.; Wu, S.; Xue, C.; Boey, F. Y. C.; Yan, Q.; Chen, P.; Zhang, H. *In Situ* Synthesis of Metal Nanoparticles on Single-Layer Graphene Oxide and Reduced Graphene Oxide Surfaces. *J. Phys. Chem. C* **2009**, *113*, 10842–10846.